THE JOURNAL OF PHYSICAL CHEMISTRY C

ARTICLE

pubs.acs.org/JPCC

IR Studies of H/D Exchange of Water, Hydroxyl, and Carboxylic Groups Reveal Slowly Diffusing Lattice Defects in Sub-Nanometer Pores

Natalia Pérez-Hernández,[*,†,⊥] Martín Febles,[‡] Cirilo Pérez,[‡] Johann Spandl,[§] Julio D. Martín,[∥] and Hans-Heinrich Limbach[*,†]

[†]Institut für Chemie und Biochemie - Physikalische und Theoretische Chemie, Freie Universität Berlin, Takusstrasse 3, D-14195 Berlin, Germany

[‡]Instituto de Bioorgánica, Universidad de La Laguna-CSIC, Ctra. Vieja de La Esperanza 2, 38206 La Laguna, Tenerife, Spain

[§]Institut für Chemie und Biochemie - Anorganische Chemie, Freie Universität Berlin, Fabeckstrasse 34/36, D-14195 Berlin, Germany

[∥]Instituto de Investigaciones Químicas, CSIC, Avda. Américo Vespucio 49, 41092 Seville, Spain

Supporting Information

ABSTRACT: We have studied the properties of a series of solid hydrated organic porous networks with pore diameters ranging from approximately 0.4 to 0.9 nm using the attenuated total reflection infrared (ATR-IR) technique. These subnanometer organic pores are composed of water and of organic racemic bicyclic monomers containing carboxylic, alcoholic, ether functions and different appendices. In particular, the doubly hydrated hydroxyl acids **1** 2H_2O and **2** 2H_2O form cylindrical pores in which half of the water molecules are part of the walls and the other half are located inside the pores. In a first step, by a comparison of the spectra of a family of related compounds, the COOH, COH as well as the wall and pore water stretches were assigned. The COOH bands are broad and red-shifted as compared to carboxylic acid dimers, and exhibit a substructure assigned to Fermi resonances. The OH stretches fulfill well Novak's correlation with the corresponding crystallographic O...O distances. In a second step, we have followed the deuteration of the different functional groups of solid **2** 2H_2O by ATR-IR by heavy water vapor. Surprisingly, we observe that the rates of deuteration are the same for all functional groups although exhibiting biexponential time dependence, in contrast to the liquid state where COOH groups exchange protons with water much faster than with alcohols. This result is rationalized in terms of slowly diffusing lattice defects resembling a local liquid or glass in the subnano scale in which the different exchange reactions take place. The nonexponential deuteration is explained in terms of a faster deuteration of crystal surface layers.

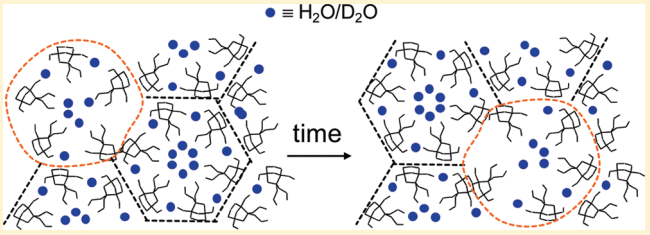

INTRODUCTION

Confined water in biological systems plays an important role for their structure, dynamics and function[1−4] Unfortunately, the complexity of biological systems makes it very difficult to obtain information about the behavior of water in locally well-defined spaces.[5−7] Therefore, the study of confined water in porous organic networks has raised significant interest in the last years.[8,9] To this aim, some of us have designed and synthesized bicyclic organic hydroxyl acids and diacids designed in such a way that they form porous hydrogen bonded networks in the solid state with pore diameters that range from approximately 0.4 to 0.9 nm. The "primary" chemical structures of these compounds are depicted in Chart 1.

All of them contain a carboxylic and an ether function, and either an additional carboxylic or alcohol function leading to extended hydrogen bonded networks in the solid state. The monomers are optically active, but the solids are racemic (±) as they are composed of alternating enantiomers. Some of the solid networks incorporate one or two water molecules per organic monomer.

X-ray diffraction[10−12] revealed interesting "secondary structures" in the solid state. The hydrogen bond pattern of **1** 2H_2O and **2** 2H_2O is depicted in Chart 2: the OH groups of the organic monomers form a hydrogen bond to the carboxyl group of an adjacent monomer, whose COOH group is bound to a water molecule which forms in turn another hydrogen bond to the ether oxygen of the first monomer. The remaining OH group of water is bound to the hydroxyl group of another adjacent monomer. **3** 2H_2O[13] is isomorphous to **1** 2H_2O and **2** 2H_2O. **6** H_2O[14] forms linear chains via cyclic hydrogen bonded acid dimers, where in each second dimer two water molecules are inserted as depicted in Chart 2. Compound **8**[14] is an anhydrous dicarboxylic acid forming a linear chain. Single crystals of compounds **4**,[15] **7** H_2O,[16] and **9**[16] were studied by X-ray crystallography, but structural-packing details were not made available in advance to the studies described herein. Although compound **5** did not afford crystals

Received: December 21, 2010
Revised: March 28, 2011
Published: April 22, 2011

Chart 1. Chemical Structures of Organic Compounds Studied in This Work[a]

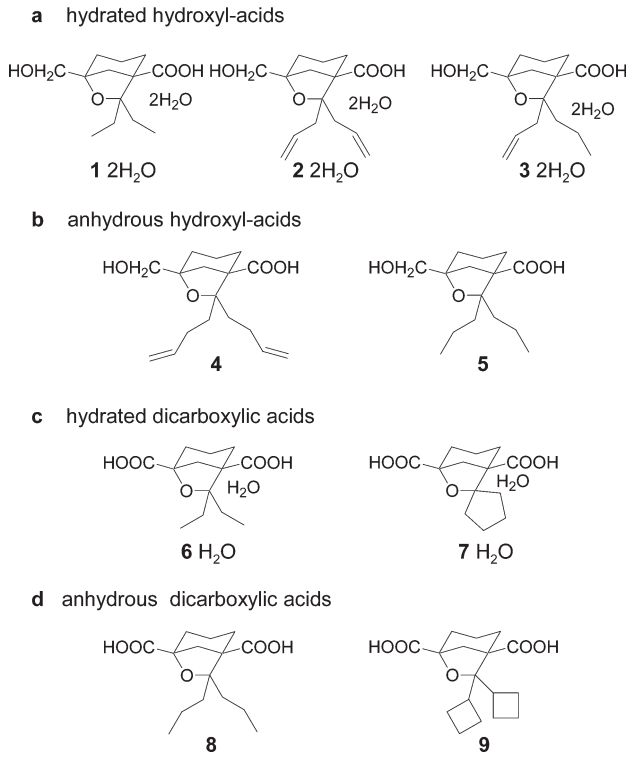

[a]The general synthetic strategy for obtaining the hydroxyl-acids is described in refs 11 and 15. The dicarboxylic acids are obtained from the oxidation of the corresponding hydroxyl-acid using the Jones reagent under standard conditions. Analytical data for **1** $2H_2O$ and **5** are described in ref 11, of **2** $2H_2O$ in ref 10, of **3** $2H_2O$ in ref 13, and of **6** H_2O and **8** in ref 14. Analytical data for compounds **4**, **7**, and **9** are described in the Supporting Information of this work.

Chart 2. Hydrogen Bond Pattern of the Solids 1 $2H_2O$,[11] 2 $2H_2O$,[10] 6 $2H_2O$,[14] and 8.[14]

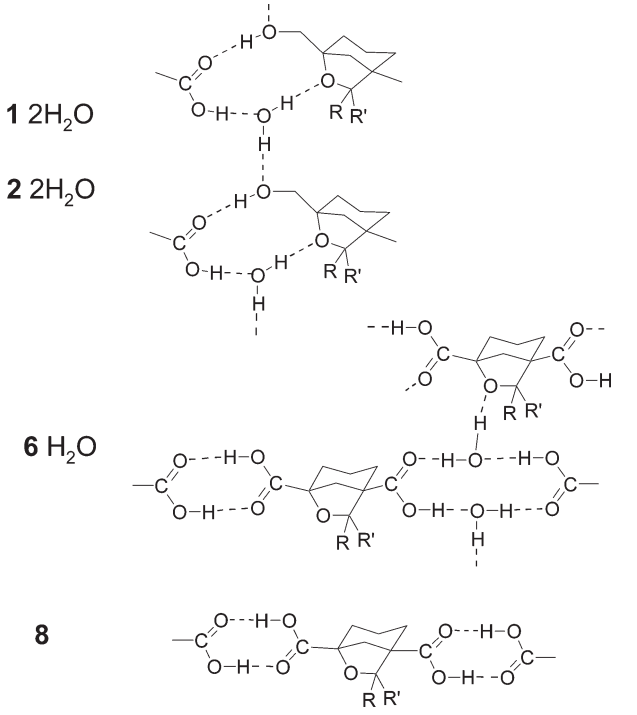

suitable for an X-ray study, thermogravimetry results show that it forms an anhydrous structure (see Supporting Information).

A desired consequence of the molecular design of the monomers is that interesting "tertiary" molecular architectures are formed in the solid state. Up to date, some of us have elucidated the tertiary structures of **1**·$2H_2O$,[11] **2**·$2H_2O$,[10] and of **6**·H_2O.[14] As illustrated in Figure 1a, in the case of the hydroxyl acids, six organic monomers form together with six water molecules (which are referred to as "wall water"), a cyclic hydrogen bonded hexamer, where several hexamers are held together by water—alcohol hydrogen bonds, resulting in the formation of subnanometer sized porous cylindrical assemblies. The pore diameter is periodically changing as illustrated in Figure 1b resulting in local "pools" containing the remaining six water molecules (which are referred to as "pore water"), per organic monomer in addition to the six water molecules in the walls.

Intrigued by the properties of both types of water some of us have studied the structure and the dynamics of confined water inside **1** $2H_2O$ and **2** $2H_2O$ using various techniques. Far infrared spectroscopy[13] indicated water bands around 500 cm^{-1} whose absorbance increased with temperature; these findings were assigned to the breaking and reformation of hydrogen bonds between water molecules. Differential scanning calorimetry[10] and ^1H and ^2H solid state NMR[10] experiments indicated a complex water structure and mobility from the microsecond to the time scale of several days. Whereas at room temperature the alcoholic and carboxylic functions are immobile within the ^2H solid state NMR time scale, water droplets were found to be very mobile, and the remaining water of the walls and the pores exchanged rapidly and was subject to a fast rotational diffusion, as found previously for ice.[17] The rotational diffusion slows down upon decreasing the temperature.

Another puzzling result was the finding that **1** $2H_2O$ and **2** $2H_2O$ could be deuterated in the mobile proton sites by exposure of the undeuterated solids to heavy water vapor.[10] Variable temperature powder X-ray diffraction and thermogravimetry[12] confirmed that water can be partially removed from the solids without destroying the crystal structures. These results prompted us to wonder about the mechanism of the diffusion of water in organic crystals which is a prerequisite of the gas—solid state deuteration process. A literature search revealed previous studies using various methods and systems which represent interesting models for various biological and pharmacological phenomena.[18−27] Up to date, the way of how water diffuses through organic crystals is not settled. Some authors invoke fast diffusion of water molecules mediated by transient fluctuations in the crystal lattices[20,21] and others small local voids in the unit cells of nonporous crystals through which water diffuses.[26] One of us found evidence for vacancies moving slowly through the crystallites where the vacancies are filled with water which exchanges mobile protons with molecules in neighboring filled sites.[25] We decided to use the previously described subnanopores to try to shed some light on this issue.

In contrast to a solid state ^2H NMR study of a dihydrated, strongly hydrogen bonded crystal where only the crystal water was deuterated but not the strong hydrogen bonds,[28] we could not resolve individual deuteratation rates of the different functional groups of **1** $2H_2O$ and **2** $2H_2O$.[10] We were intrigued by

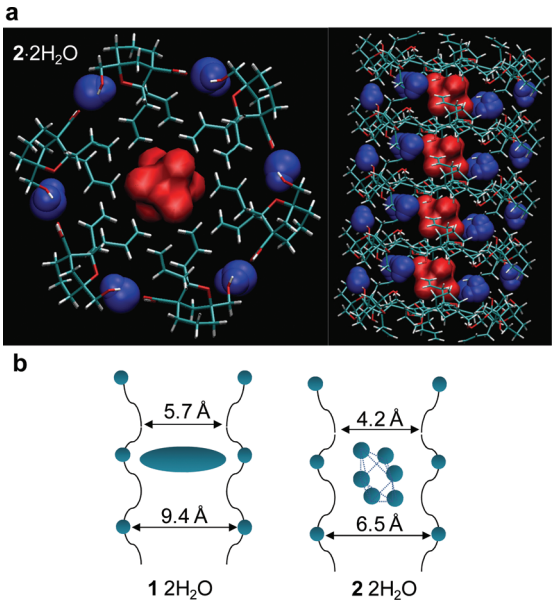

Figure 1. (a) Crystal structure of **2**·2H_2O according to ref 10. A similar structure is adopted by **1** 2H_2O.[11] (b) Schematic pore profile of compounds **1** 2H_2O and **2** 2H_2O. Blue spheres represent water molecules. Typical average diameter sizes are indicated. The water inside the pore in **1** 2H_2O is diffuse (blue flat ellipse) and less structured than in **2** 2H_2O, where it is represented by individual spheres.

this finding and thought that knowledge of the individual rates could provide additional information about the mechanism of the gas/solid state deuteration and the diffusion of water through crystals. We thought that the method of choice to solve this problem would be attenuated total reflection infrared (ATR-IR) spectroscopy of the pure polycrystalline powders which would allow us to follow the different OH-stretching bands as a function of the time of exposure to heavy water vapor. We did not take solution spectra, as the supramolecular structures, object of this study, break down as shown in previous work by some of us.[29]

In order to achieve our goal, we first needed to assign the OH stretching bands of the different functional OH groups. This task was not easy but we succeeded by comparing the ATR IR spectra of the series of solid compounds depicted in Chart 1. In a second stage, we followed the gas phase deuteration of **2** 2H_2O as a function of time. Surprisingly, the outcome of our study is that no preferential deuteration site was identified. Together with the NMR results concerning the rotational diffusion of water, this finding enabled us to derive a scenario for water diffusion and deuteration via a slow diffusion of local defects through the crystal lattice of the subnanopores.

EXPERIMENTAL SECTION

ATR-IR (attenuated total reflection infrared) spectra[30] of the polycrystalline organic solids in Chart 1 were measured in diffuse reflection using a Nicolet Nexus-FT-IR spectrometer 670 equipped with a SMART DuraSamplIR diamond attenuated total reflection (ATR) accessory. The resolution was 4 cm^{-1} and the number of scans 200. About 1−2 mg of the solid materials was used for each measurement.

The time dependence of the solid state deuteration of **2** 2H_2O was measured as follows. Approximately 25 mg aliquots of the polycrystalline compound were exposed to heavy water vapor in a small closed desiccator that contained approximately 20 mL of liquid D_2O at the bottom. The system was then put inside an oven at 45 °C. Samples were taken out at various exposure times and immediately measured. The corresponding spectra (Figure 3) are normalized to the intensities of the nondeuterated CH stretching bands.

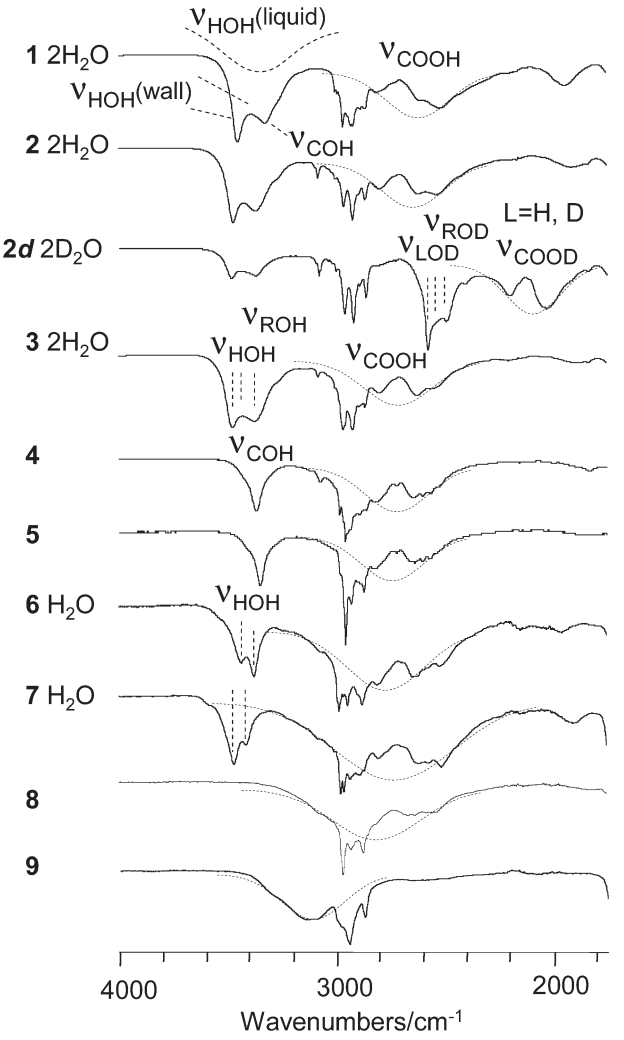

Figure 2. ATR-IR spectra of various solid hydrated or anhydrous hydroxyl acids or diacids. Included are spectra of **2** 2H_2O before and after exposure to heavy water vapor at 45 °C for 7 days leading to the deuterated isotopolog ***2d*** 2D_2O. The dashed band included at the top between 3300 and 3400 cm^{-1} represents the experimental IR stretch of pure liquid water at 289 K adapted from ref 29. The dashed Gaussian bands below 3200 cm^{-1} indicate the envelope of the carboxylic stretch ν_{COOH}. For further explanation see text.

RESULTS

In Figure 2 are depicted the ATR-IR spectra of the compounds of Chart 1, including a spectrum of a sample labeled as ***2d*** 2D_2O, obtained by partial deuteration of **2** 2H_2O using heavy water vapor. We did not try to analyze the aromatic and aliphatic CH stretches above and below 3000 cm^{-1} as our interest focused on the OH stretches. The comparison of the different systems allowed us to identify the different bands. Their frequencies are collected in Table 1 together with assignments and known O···O distances as discussed in the next section.

dx.doi.org/10.1021/jp112105j |J. Phys. Chem. C 2011, 115, 9393–9402

Table 1. Assignments and Wave Numbers of the Infrared OH Stretching Bands of Solid Hydroxyl Acids and Diacids

compound	band center (cm^{-1})	subbands cm^{-1} maxima	subbands cm^{-1} minima	assignment	X-ray structure	H bond	d(O···O) (Å)
1 $2H_2O$	3453			ν_{H2O}	ref 11, RT	HOH···O-H	2.753
	3393[b]			ν_{H2O}		HOH···O<	2.712
	3317			ν_{COH}		OH···O=C	2.711
	2600[a]	2518	2583	ν_{COOH}		COOH···OH_2	2.563
		2613	2707				
		2808					
2 $2H_2O$	3472			ν_{H2O}	ref 10, 170 K	HOH···O-H	2.772
	3412[b]			ν_{H2O}		HOH···O<	2.749
	3365			ν_{COH}		OH···O=C	2.790
	2650[a]	2534		ν_{COOH}		COOH···OH_2	2.602
		2619	2583				
		2796	2708				
2 2 L_2O L = H,D	2571			ν_{D2O}		LOD···O-L	
	2527[c]			ν_{D2O}		LOD···O<	
	2482			ν_{COD}		OD···O=C	
	2080[a]	2031	2125	ν_{COOD}		COOD···OL_2	
		2202					
3 $2H_2O$	3474			ν_{H2O}		HOH···O-H	
	3427[b]			ν_{H2O}		HOH···O<	
	3369			ν_{COH}		OH···O=C	
	2675[a]	2453		ν_{COOH}		COOH···OH_2	
		2622	2576				
		2799	2708				
4	3366			ν_{COH}			
	2700[a]	2528		ν_{COOH}			
		2558	2540				
		2598	2580				
		2644	2613				
		2811	2720				
5	3350			ν_{COH}			
	2710[a]	2533		ν_{COOH}			
		2564	2549				
		2601	2579				
		2634	2616				
		2662	2647				
		2826	2720				
6 H_2O	3436			ν_{H2O}	ref 14	HOH···O=C	2.852
	3375			ν_{H2O}		HOH···O<	2.800
	2775[a]	2515	2546	ν_{COOH}		COOH···O=C	2.652
		2634	2701			COOH···OH_2	2.599
		2805					
7 H_2O	3468			ν_{H2O}			
	3409			ν_{H2O}			
	2725[a]	2509	2546	ν_{COOH}			
		2570	2589				
		2619	2714				
		2805					
8	2800[a]	2558	2604	ν_{COOH}	ref 14	COOH···O=C	2.664
		2653	2735				
		2808					
9	3125[a]	3125	3125 max	ν_{COOH}			

[a] The COOH stretching bands are broad and exhibit a substructure spread through the spectra showing several peaks; the value that appears in the table is the maximum of a simulated Gaussian band. [b] Values estimated using a frequency shift of 60 cm^{-1} as observed for **6** H_2O and 7 H_2O. [c] Value estimated using a frequency shift of 60/1.35 cm^{-1} as described in the text.

dx.doi.org/10.1021/jp112105j |*J. Phys. Chem. C* 2011, 115, 9393–9402

Alcoholic OH Stretching Bands. The simplest OH vibrations to assign were the alcoholic stretches ν_{COH}. They give rise to relatively sharp bands without fine structure around 3360 cm^{-1} as can be clearly seen in the case of the anhydrous hydroxyl acids **4** and **5**. These bands help to identify the corresponding bands of the doubly hydrated hydroxyl acids **1** 2H_2O, **2** 2H_2O, and **3** 2H_2O. Only in the case of **1** 2H_2O ν_{COH} is slightly red-shifted.

Water OH Stretching Bands. The hydrated diacids **6** H_2O and 7 H_2O show that water molecules contribute a pair of OH stretching bands labeled as ν_{H2O} around 3400 cm^{-1} to the ATR IR spectra. The two bands are separated by 60 cm^{-1}. Later, we will discuss whether these bands correspond to the antisymmetric and symmetric OH stretches of water exhibiting C_{2v} symmetry, or to two inequivalent local OH stretches.

In the case of the hydrated hydroxyl acids that form the subnanopores only the high-frequency band can be clearly distinguished in the OH stretching region because of spectral overlap with ν_{COH}. We assign this band to the high-frequency OH stretch of wall water representing 50% of all water molecules in the samples. We assume that the second water band is also red-shifted by 60 cm^{-1} in analogy to **4** and **5**. Thus, this band will appear in the gap between the high frequency band and ν_{COH} as illustrated in Figure 2. However, we expect in the same region the stretches of the second half of the water molecules, the pore water. For comparison, we have added at the top of Figure 2 a dashed curve representing the experimental IR band of pure liquid water at 289 K.[31d] The maximum of this band appears around 3350 cm^{-1} and its half-width is about 300 cm^{-1}. As will be discussed later, we think that the pore water contributes a similar band to the spectra of the hydrated hydroxyl acids.

COOH Stretching Bands. The COOH stretches, labeled as ν_{COOH}, give rise to broad bands. In each spectrum in Figure 2, the dashed curve is a simulation of these broad bands. As demonstrated in the case of the dehydrated diacid **9** by the corresponding dashed curve, the band shape is close to a Gaussian, the band maximum appearing at 3125 cm^{-1} and the bandwidth being about 500 cm^{-1}. Not only red-shifts, but also more complicated band structures exhibiting several maxima and minima are observed for the other compounds. The corresponding frequencies as well as those of the assumed band maxima calculated from the dashed bands in Figure 2 are included in Table 1. The origin of this complex band structure will be discussed in the next section.

Deuteration of Solid 2 2H_2O by Heavy Water Vapor. We have included in Figure 2a spectrum of a sample of **2** 2H_2O which had been exposed for 7 days to heavy water vapor. We labeled the new sample as ***2d*** 2D_2O although only partial deuteration has occurred to about 60%. Similar spectra (Supporting Information, Figure S1, B) were obtained when **2** 2H_2O was deuterated by repeated (3 times) dissolution and evaporation in CH_3OD, and crystallization of the solid residue from a non polar solvent (CCl_4) saturated in liquid D_2O. We will comment this result in the Discussion section.

In the spectrum of ***2d*** 2D_2O in Figure 2, the intensities of the ν_{H2O} and ν_{COH} around 3400 cm^{-1} have been reduced to about 40% of its original value, but the band shape did not change. A new broad band labeled as ν_{COOD} has appeared around 2000 cm^{-1}, exhibiting only a single minimum. The ν_{COOH} band around 2650 cm^{-1} has mostly disappeared, in particular the left subband with the maximum at 2796 cm^{-1}, and at 2571 cm^{-1} a ν_{D2O} band and at 2482 cm^{-1} a ν_{COD} have appeared. Their band shape resembles the one of ν_{H2O} and ν_{COH}, as it contains the second water band, it is reduced by about 1.4 as expected from the mass changes. The band frequencies are included in Table 1, from which it follows that the ratios ν_{H2O}/ν_{D2O} and ν_{COH}/ν_{COD} are about 1.35, whereas the ratio ν_{COOH}/ν_{COOD} is 1.27. Using this information, we assign a frequency of 2527 cm^{-1} to the second vibration ν_{D2O}, shifted by 60/1.35 cm^{-1} from the first.

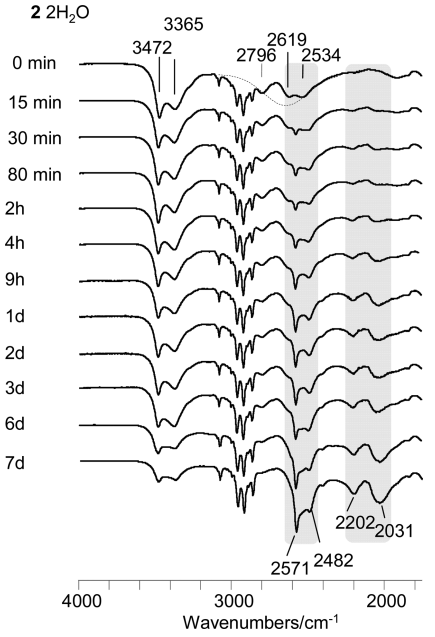

Figure 3. ATR-IR Infrared spectra of **2** 2H_2O exposed for different times to D_2O vapor at 45 °C as described in the experimental section.

In Figure 3 are depicted the ATR IR spectra of **2** 2H_2O as a function of the time of exposure to heavy water vapor in a closed recipient at 45 °C. The vials containing the samples were carefully closed right before registering each ATR-IR spectrum, which was done immediately afterward placing approximately the same amount of each sample in the spectrometer.

In order to obtain information about the time dependence of the protonated and deuterated species we normalized the spectra to the CH stretching bands and plotted the intensities of the left ν_{H2O} band at 3472 cm^{-1}, of the ν_{COH} band at 3365 cm^{-1}, and of the ν_{COOD} band at 2024 cm^{-1} as a function of time as illustrated in Figure 4. We observe an initial rapid decay of the H content; then, it seems that the H content does not change or even increases somewhat before it further decays. We associate this behavior with a large margin of error of our data, and not to a real intermediate increase of the H content which is unlikely. Because of the large margin of error, we simulate the data in terms of a biexponential decay, although the latter may be multiexponential.

The intensities at $t = 0$ were set to 1 in the first two cases, leading to a value of 0.4 at $t = 7$ d, indicating a H content of 40%. Therefore, we normalized the intensities of the ν_{COOD} band to a value of 0.6 at $t = 7$ d. The data in Figure 4, panels a and b, were fitted to a biexponential decay

$$A = A_1 \exp(-t/T_1) - (1 - A_1) \exp(-t/T_2) \quad (1)$$

and those of Figure 4c to a biexponential growth

$$A = 1 - A_1 \exp(-t/T_1) - (1 - A_1) \exp(-t/T_2) \quad (2)$$

The solid lines were all calculated using the same data set with $A_1 = 0.25$, $T_1 = 0.1$ d, and $T_2 = 16$ d.

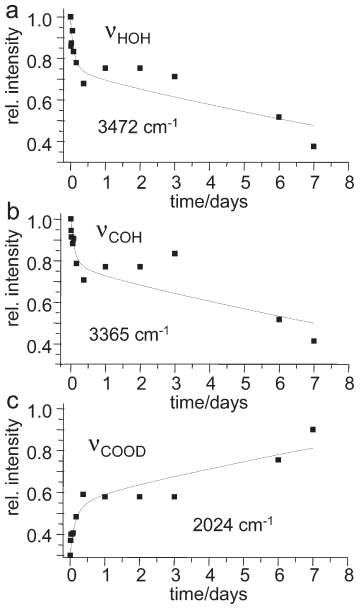

Figure 4. Intensities of selected bands of the spectra as a function of the time of exposure of the crystalline solid **2** $2H_2O$ to heavy water vapor at 45 °C. The solid lines were calculated as described in the text.

DISCUSSION

ATR IR Band Assignments. By comparison of the ATR IR spectra of all compounds in Chart 1, we were able to assign all OH stretching bands and the results were included in Table 1.

Water OH Stretching Bands. The hydrated diacids **6** H_2O and **7** H_2O gave rise to two water stretching bands around 3400 cm^{-1}, spaced by 60 cm^{-1}. At first sight, it is tempting to assign the higher frequency band to the antisymmetric stretch ν_3 and the lower frequency band to the symmetric stretch ν_1 of water exhibiting $C_{2\nu}$ symmetry. Alternatively, the water symmetry could be lifted leading to two localized OH stretching vibrations.

Usually, ν_1 represents only about 1/3 of the intensity of ν_3.[32] This feature is well fulfilled for **7** H_2O but not for **6** H_2O as depicted in Figure 2. Schiffer et al.[33] have reported a linear correlation between the average stretching frequency $\nu_{OH} \approx {}^1/_2(\nu_1(H_2O) + \nu_3(H_2O))$ and the splitting between the antisymmetric and symmetric OH stretching bands of water exhibiting $C_{2\nu}$ symmetry

$$\nu_3 - \nu_1 = 0.2975\nu_{OH} - 669.2\ cm^{-1} \qquad (3)$$

from which we calculate a line splitting of about 40 cm^{-1}. The value of 60 cm^{-1} found here for **6** H_2O and **7** H_2O is clearly outside the margin of error of eq 3. Finally, in the case of water exhibiting C_{2v} symmetry, new OH and OD stretching bands should appear upon partial deuteration, arising from HDO appearing at ν_{OH} and at $\nu_{OD} \approx {}^1/_2(\nu_1(D_2O) + \nu_3(D_2O))$.[34] This leads to typical band shape changes, which are, however, absent in the deuteration studies of **2** $2H_2O$ as illustrated in Figure 3. Therefore, we opt for the explanation that the symmetry of H_2O in the hydroxyl acids and diacids studied is reduced and that the two OH oscillators are inequivalent. As the low-frequency water band is not well resolved in the case of the hydrated hydroxyl acids, we estimated that the frequency shift between the two water bands in these compounds is also about 60 cm^{-1}, as indicated in Table 1. This inequivalence is supported by the finding of unequal O···O distances of the two hydrogen bonds in the crystal structures of the hydrated hydroxyl acids (Table 1) in which half of the water molecules, those in the walls, are engaged.

However, these considerations only refer to one-half of all water molecules of the hydrated hydroxyl acids, i.e., to the wall water molecules in defined crystallographic sites. The OH stretches of the other half, those in the pores, can be assigned by comparison with the OH stretching band of pure water[31d] included at the top of Figure 2 as dashed curve. This band is centered at 3350 cm^{-1} and exhibits a width of about 300 cm^{-1}. Pore water gives rise to a similar band in the spectra of the hydrated hydroxyl acids; it fills partially the gap between the high-frequency wall water and the alcoholic stretching bands, and gives rise to the broad shoulder at 3430 cm^{-1}. This broad band, in particular the shoulder, is absent in the spectra of the anhydrous hydroxyl acids and the diacids.

For comparison, OH stretching frequencies of water in other organic and metal−organic frameworks[35,36] appear as broad bands at two frequencies similar to the values observed in the present paper. On the other hand, the stretching frequencies of free hydroxyl groups have been calculated to exhibit frequencies higher than 3500 cm^{-1}.[37] This discards the presence of non H-bonded OH groups in our samples. It has not been possible to assign a clear O···O distance for the pore water molecules present in **1** $2H_2O$ and **2** $2H_2O$ by means of X-ray diffraction. The fact that we do not observe a free OH stretching band indicates that every OH group of the pore water is involved in hydrogen bonding. Neutron diffraction experiments planned for the close future will hopefully clarify this point.

COOH Stretching Bands. As mentioned in the previous section, the typical broad line shape of ν_{COOH} is best seen in the case of **9** where this band is shifted to the high frequency side of the CH stretching bands. In the other cases the band experiences a red shift, in agreement with a shortening of the O···O hydrogen bond distances.[38] The red shift is accompanied by the occurrence of several maxima and minima within the expected envelope of ν_{COOH} illustrated by the dashed Gaussian lines in Figure 2. Similar features have been observed by Ratajczak et al. for matrix-isolated trifluoroacetic acid-dimethyl ether (TFA-DME) complexes.[39] The minima correspond to "Evans holes"[40] arising from Fermi resonances between the OH stretches and lower-lying frequencies. In the case of TFA-DME the minima were assigned to the interaction with the overtone of the bending vibration $2\delta_{COOH}$ and with the combination $\nu_{C-O} + \delta_{COOH}$. As we find a minimum in the ν_{COOD} band of ***2d*** $2H_2O$ (Figure 2) we assume that the in-plane bending vibration contributes to the origin of the Fermi resonances observed. The fact that the ν_{COOH} band of **9** does not exhibit a substructure is in agreement with this interpretation, as this band is blue-shifted so that the resonance condition is no longer fulfilled.

In order to support this interpretation we checked the fingerprint region of the full ATR-IR spectra (Figure S1 of the Supporting Information) for H/D isotope sensitive bands. Although we observe spectral changes for **2** $2H_2O$ around 1300 cm^{-1} upon deuteration, we were not able to identify δ_{COOH}. This is not surprising as the determination of the in-plane bending vibrations is often difficult because of strong coupling to skeleton and lattice modes.[38,41] Around 960 cm^{-1} we observe a sharp band which disappears upon deuteration, and

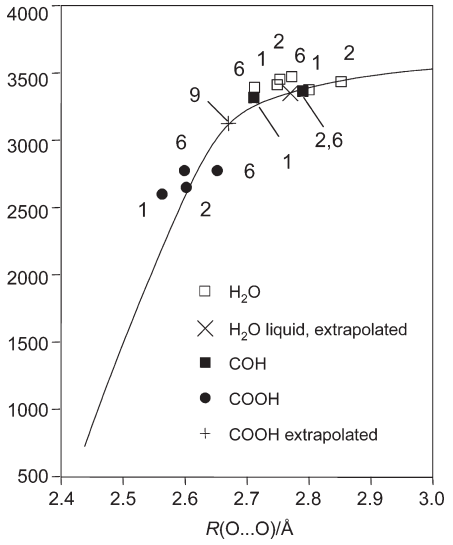

Figure 5. Hydrogen bond correlation between OH stretching frequencies and O···O distances of compounds **1** $2H_2O$, **2** $2H_2O$ and **6** $2H_2O$ abbreviated as **1**, **2** and **6**. An O···O distance of 2.67 Å is obtained for the COOH···O hydrogen bonds of **9** by placing the frequency value measured on the solid correlation curve proposed by Novak.[38]

a new band appears at 750 cm^{-1} (see the Supporting Information). We tentatively assign these bands to the out of plane bending vibrations γ_{COOH} and γ_{COOD}. These values are in agreement with the correlation between OH-stretching and out of plane bending vibrations proposed by Novak.[38]

Hydrogen Bond Correlation between OH Stretching Frequencies and O···O Distances. Several correlations between the OH stretching vibration frequencies and the O···O distance in O—H···O hydrogen bonds have been reported.[38,42] As the X-ray structures of some of the compounds are available (Table 1), we have plotted in Figure 5 the observed OH stretching frequencies of these compounds as a function of the corresponding O···O distances. Within the margin of error, the data obtained are well located on the solid correlation curve proposed by Novak.[38] The COOH stretching frequency of compound **9** was placed on the correlation curve leading to an O···O distance of 2.67 Å. We hope that this value may be checked in the future by crystallographic studies.

We have included in Figure 5a data point for liquid water exhibiting a stretching frequency of 3350 cm^{-1}, indicating an O···O distance of about 2.77 Å. This value is in good agreement with experimental and calculated data of liquid water.[43]

Mechanism of the Deuteration of the Subnanopore Formed by 2 $2H_2O$ by Heavy Water Vapor. In this section, we discuss the mechanism of deuteration of the mobile proton sites of crystalline **2** $2H_2O$ by gaseous D_2O. In previous related cases of cyclodextrins,[18−21] calixarenes[26] and sugars,[27] where only alcoholic groups were deuterated, the conclusions about the reaction mechanism remained vague. Here, we obtain more precise information in the case of crystalline **2** $2H_2O$ because of the presence of different functional groups, i.e., partially ordered water in the main subnanopores, ordered crystalline water molecules in the molecular network, and the carboxyl and alcoholic groups. The following discussion will also be valid for **1** $2H_2O$ whose gas phase deuteration was detected previously using NMR[10] and for crystalline **3** $2H_2O$.

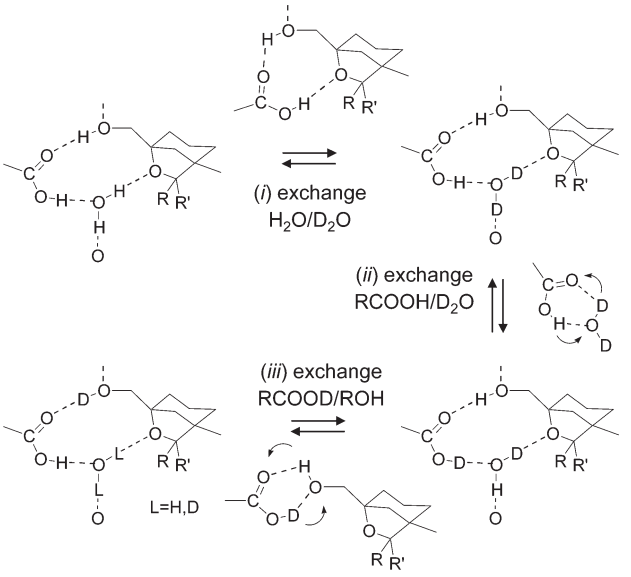

Figure 6. Mechanism of deuteration of the crystalline subnanopores formed by the hydrated hydroxyl-acids depicted in Chart 1a. First step: Replacement of H_2O by D_2O via a water vacancy. Second step: H/D exchange in a cyclic hydrogen bonded COOH/D_2O complex formed in a hydroxyl acid vacancy. Third step: H/D exchange in a cyclic hydrogen bonded COOD/COH complex formed in a water vacancy followed by reinsertion of a water molecule L_2O, L = H, D.

Figure 6 provides an overview of the deuteration process of the crystalline hydrated hydroxyl acids observed in this study, which consists in fact of three subsequent reactions, consisting each of different steps: (i) entrance of gaseous D_2O into the pores of **1** $2H_2O$ and replacement of H_2O in the solid frame by the incoming D_2O, (ii) hydron exchange between water and the carboxyl groups, and (iii) hydron exchange between carboxyl groups and alcohol groups. Exchange between COOH and OH groups has been well established to proceed in cyclic 1:1 hydrogen bonded intermediates.[45,46] By contrast, proton exchange between alcohol groups cannot take place directly but requires the presence of acid or basic impurities.[44]

All of these reactions take place in the polycrystalline solid. However, they all require a certain rotational and translational mobility of the reaction partners, a conclusion which is not in agreement with periodically arranged unit cells as observed by X-ray crystallography.

The kinetic results described in Figure 4 showed as a surprise that all mobile proton sites experience the same rate coefficient of deuteration, in spite of their different chemical structures. Usually, in the liquid state, the rate of proton exchange between alcoholic OH groups is slow, even in pure methanol.[44] By contrast, proton exchange between carboxylic groups and alcoholic groups is fast and involves a concerted double proton transfer proceeding by tunneling.[45,46]

A second important result of Figure 4 is that 1/4 to 1/3 of the OH groups are deuterated much faster than the remaining ones. Similar results have been observed previously in the case of the deuteration of solid sugars containing alcoholic OH groups.[27] This finding was explained with a faster rate of deuteration of the surface layers of the crystallites, an interpretation with which we completely agree. On the other hand, when fully deuterated samples ***2d*** $2D_2O$ are prepared by crystallization from D_2O, rapid surface reprotonation can occur by moisture during the sample

dx.doi.org/10.1021/jp112105j |J. Phys. Chem. C 2011, 115, 9393–9402

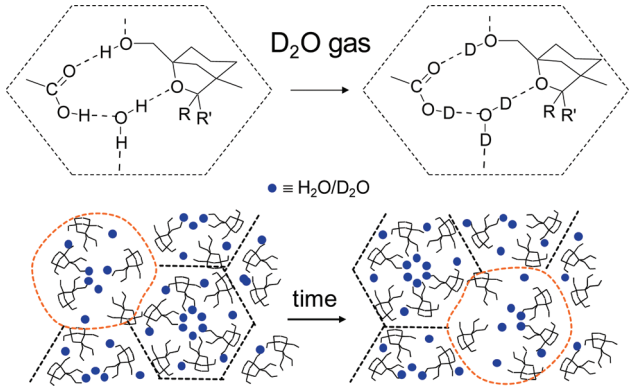

Figure 7. Scenario of the diffusion of disordered vacancies or other defects. Mechanism of the deuteration of the crystalline subnanopores formed by hydrated hydroxyl acids.

transfer to the spectrometer, as demonstrated by Figure S1 B in the Supporting Information. A similar process may also be the reason why the ATR IR spectra still contain substantial amounts of protonated species even after prolonged exposure to heavy water vapor in a desiccator as illustrated in Figure 3.

Diffusion of Lattice Defects As Rate Limiting Step of the Deuteration of the Subnanopore Formed by 2 $2H_2O$. The finding that the rates of H/D exchange of the different functional groups in **2** $2H_2O$ are the same indicates that the rate limiting step of the deuteration is not the proton exchange itself, but another very slow process such as the presence of vacancies or defects which diffuse slowly through the individual crystallites. Such defects and their diffusion have well been established using various techniques as reviewed by Sherwood.[47]

One of us has studied the deuteration of solid porphyrin[25] by heavy water vapor; in this solid there are no channels in which water could move. Therefore, it was proposed that there are vacant crystallographic sites filled with water, which slowly move through the crystal and exchange deuterons with porphyrin molecules.

Here, we invoke a similar mechanism for the lattice defect diffusion and associated deuteration of hydrated hydroxyl acids by water vapor. The formation of water vacancies in the walls is favored by entropy: when water molecules leave the wall sites and join sites in the pores entropy strongly increases because the pores have free space available leading to a large number of possible water arrangements. A related situation was found previously for pyridine in mesoporous silica,[48] where the pyridine molecules are either bound to surface SiOH groups or in a bulk pore phase. The formation of the latter is entropy driven even in the case of a monolayer. Water vacancies create space in the walls which may induce in turn also vacant sites of the organic constituents.

The molecular scenario of lattice defect diffusion we have in mind is illustrated schematically in Figure 7. Any deviation from the unit cell geometry will represent a lattice defect, but the reactions of Figure 6 require larger defects, typically of the order of a unit cell. We speculate that such a defect will resemble more a local subnano-liquid or subnano-glass containing vacancies and mobile crystal constituents. In such a lattice defect all mobile proton sites, water, alcoholic and carboxylic sites will exchange rapidly their protons one after the other as discussed above, enabling deuteration when water is replaced by heavy water. Whereas formation and translational diffusion of either water vacancies or organic hydroxyl acid vacancies determines how fast the deuteration zone moves through the crystal lattice, rotational diffusion processes will determine the rate of deuteration within a lattice defect. However, once a lattice defect is created, molecular motions are accelerated, and hence translational diffusion will be in fact the rate determining step. Nevertheless, let us rediscuss the reactions depicted in Figure 6, but now taking into account the confinement in the crystal.

For reaction (i), first a water molecule must leave the site in which it was bound, leaving a water vacancy. As the hydrogen bond network is perturbed, it is conceivably that the two adjacent organic molecules approach somewhat and that the COOH group of one molecule forms a hydrogen bond with the ether oxygen of the second molecule. In the next step, a D_2O molecule is bound.

In reaction (ii) one organic molecule must break the two hydrogen bonds to the adjacent water and the adjacent organic molecule. It is difficult to know whether the latter stays nearby or whether it involves the formation of a vacant organic site. We note that slowly moving vacancies are common in organic solids.[49,50] Anyway, this heavy atom motion enables the formation of a cyclic 1:1 complex between the carboxylic group and one water molecule. In such a complex, a fast degenerate double proton transfer takes place.[45,46] The original proton position is then restored by a 180° flip of the carboxylic−water moiety. We note that related flips have been observed by ^{17}O NMR in solid $(COOH)_2$ units of solid dimethylmalonic acid.[51] After the reforming of the original hydrogen bond network and the repetition of reactions (i) and (ii), a situation is achieved where all water and carboxylic sites are deuterated, but not yet the alcoholic sites.

The latter are then deuterated in reaction (iii). For that process to occur, first a water vacancy has to be created between two adjacent **1** molecules. The latter must then form a cyclic 1:1 hydrogen bonded complex in which deuteration is achieved via a fast double hydron transfer.

■ CONCLUSIONS

We arrive at the following conclusions of our ATR-IR study of organic subnanometer sized porous networks constructed from bicyclic organic hydroxyl acids (Chart 1).

The two OH oscillators of the water in the walls of the networks are nonequivalent due to different hydrogen bonds in which they are involved and contribute two stretching bands to the IR spectra between 3400 and 3300 cm^{-1}. Pore water contributes a broad band in the same region, similar to the bands of liquid water. The hydroxyl groups contribute a single band in the same region. The broad bands of COOH hydrogen bonded to water appear around 2600 cm^{-1}. The bands exhibit a substructure assigned to Fermi resonances, probably arising from overtones or combination bands involving OH bending vibrations. The band frequencies are in agreement with previously published hydrogen bond correlations.

When the solid subnanopores formed by the hydrated hydroxyl acids are exposed to heavy water vapor the four functional groups, i.e. pore water, wall water, hydroxyl and carboxyl groups are deuterated with similar reaction rates. The deuteration kinetics followed by IR is nonexponential. A fast component is ascribed to the deuteration of surface layers and the slower components to the cores of the mini crystals. In previous studies only the deuteration of single types of OH groups in nonporous

crystals by heavy water vapor[19,20,26,27] had been studied which was interpreted in terms of diffusion of water molecules through permanent or temporary lattice and molecular voids. The present observation of similar deuteration rates for all functional groups of the hydroxyl acids studied here is compatible only with larger molecular motions involving a lattice defect diffusion mechanism as illustrated schematically in Figure 7, where the lattice defects correspond to subnano-liquid glassy regions typically of the size of a unit cell.

The elucidation of this mechanism represents a contribution to the knowledge of how diffusion proceeds in crystalline samples and a confirmation of former not completely clear interpretations. It has been possible due to the systematic study of compounds with different functional groups but otherwise very similar chemical structures.

■ ASSOCIATED CONTENT

Supporting Information. Full ATR-IR spectra of the compounds of Chart 1 including **2*d*** $2D_2O$ as well as analytical data of compounds **4**, **7**, and **9**. This material is available free of charge via the Internet at http://pubs.acs.org.

■ AUTHOR INFORMATION

Corresponding Author

*E-mail: natalia.perez@iiq.csic.es; limbach@chemie.fu-berlin.de.

Present Addresses

⊥Instituto de Investigaciones Químicas, CSIC, Avda. Américo Vespucio 49, 41092, Seville, Spain.

■ ACKNOWLEDGMENT

The financial support from the Spanish Ministry of Science and Technology (MST/FEDER, project CTQ2007-61024/BQU), of the Deutsche Forschungsgemeinschaft, Bonn, Germany and of the Fonds der Chemischen Industrie, Frankfurt, is gratefully acknowledged . N.P.H. thanks the Ramón Areces Foundation for a postdoctoral grant.

■ REFERENCES

(1) Ball, P. *Nature* **2008**, *452*, 291–292.
(2) Chaplin, M. *Nat. Rev. Mol. Cell Biol.* **2006**, *7*, 861–866.
(3) Agre, P. *Angew. Chem., Int. Ed.* **2004**, *43*, 4278–4290.
(4) Water in Biological Systems (special issue). *Phys. Chem. Chem. Phys.* **2010**, *11*, 10145−10278.
(5) Ren, G.; Reddy, V. S.; Cheng, A.; Melnyk, P.; Mitra, A. K. *Proc. Natl. Acad. Sci. U.S.A.* **2001**, *98*, 1398–1403.
(6) Murata, K.; Mitsuoka, K.; Hirai, T.; Walz, T.; Agre, P.; Heymann, J. B.; Engel, A.; Fujiyoshi, Y. *Nature* **2000**, *407*, 599–605.
(7) Preston, G. M.; Carroll, T. P.; Guggino, W. B.; Agre, P. *Science* **1992**, *256*, 385–387.
(8) Water − from Interfaces to the Bulk (special issue). *Faraday Discuss.* **2009**, *141*, 1−488.
(9) Water at Molecular Interfaces (special issue). *ChemPhysChem* **2008**, *9*, 2859−2879.
(10) Febles, M.; Pérez-Hernández, N.; Pérez, C.; Rodríguez, M. L.; Foces-Foces, C.; Roux, M. V.; Morales, E. Q.; Buntkowsky, G.; Limbach, H. H.; Martín, J. D. *J. Am. Chem. Soc.* **2006**, *128*, 10008–10009.
(11) Carrasco, H.; Foces-Foces, C.; Pérez, C.; Rodríguez, M. L.; Martín, J. D. *J. Am. Chem. Soc.* **2001**, *123*, 11970–11981.
(12) Pérez-Hernández, N.; Falcao, E. H. L.; Pérez, C.; Fort, D.; Martín, J. D.; Eckert, J. *J. Phys. Chem. B* **2010**, *114*, 5694–5699.
(13) Pérez-Hernández, N.; Luong, T. Q.; Pérez, C.; Martín, J. D.; Havenith, M. *Phys. Chem. Chem. Phys.* **2010**, *12*, 6928–6932.
(14) Pérez, C.; Rodríguez, M. L.; Foces-Foces, C.; Pérez-Hernández, N.; Pérez, R.; Martín, J. D. *Org. Lett.* **2003**, *5*, 641–644.
(15) Pérez-Hernández, N.; Febles, M.; Pérez, C.; Pérez, R.; Rodríguez, M. L.; Foces-Foces, C.; Martín, J. D. *J. Org. Chem.* **2006**, *71*, 1139–1151.
(16) Compounds **7** and **9** were obtained by oxidation of the corresponding hydroxyl-acids as described byFoces-Foces, C.; Rodríguez, M. L.; Febles, M.; Pérez, C.; Martín, J. D. *Acta Crystallogr.* **2005**, *C61*, o339–o342.
(17) Wittebort, R. J.; Usha, M. G.; Ruben, D. J.; Wemmer, D. E.; Pines, A. *J. Am. Chem. Soc.* **1988**, *110*, 5668–5671.
(18) Salsa, T.; Veiga, F.; Teixeira-Dias, J. J. C.; Pina, M. E. *Drug Dev. Ind. Pharm.* **2003**, *29*, 289–297.
(19) Moreira da Silva, A.; Steiner, T.; Saenger, W.; Empis, J.; Teixeira-Dias, J. J. C. *Chem. Commun.* **1997**, 465–466.
(20) Steiner, T; Koellner, G. *J. Am. Chem. Soc.* **1994**, *116*, 5122–5128.
(21) Steiner, T.; Moreira da Silva, A. M.; Teixeira-Dias, J. J. C.; Mueller, J.; Saenger, W. *Angew. Chem., Int. Ed.* **1995**, *34*, 1452–1453.
(22) Clarke, H. D.; Arora, K. K.; Bass, H.; Kavuru, P.; Ong, T. T.; Pujari, T.; Wojtas, L.; Zaworotko, M. J. *Cryst. Growth. Des.* **2010**, *10*, 2152–2167.
(23) Gillon, A. L.; Feeder, N.; Davey, R. J.; Storey, R. *Cryst. Growth. Des.* **2003**, *3*, 663–673.
(24) Infantes, L.; Motherwell, S. *CrystEngComm* **2002**, *4*, 454–461.
(25) Braun, J.; Koecher, M.; Schlabach, M.; Wehrle, B.; Limbach, H. H.; Vogel, E. *J. Am. Chem. Soc.* **1994**, *116*, 6593–6604.
(26) Thallapally, P. K.; Lloyd, G. O.; Atwood, J. L.; Barbour, L. J. *Angew. Chem., Int. Ed.* **2005**, *44*, 3848–3851.
(27) Ahlquist, M. U. A.; Taylor, L. S *J. Pharm. Sci.* **2002**, *91*, 690–698.
(28) Klug, C. A.; Lee, P. L.; Lee, I. S. H.; Kreevoy, M. M.; Yaris, R.; Schaefer, J. *J. Phys. Chem. B* **1997**, *101*, 8086–8091.
(29) Pérez-Hernandez, N.; Pérez, C.; Rodríguez, M. L.; Foces-Foces, C.; Tolstoy, P. M.; Limbach, H. H.; Morales, E. Q.; Pérez, R.; Martín, J. D. *Bioorgan. Med. Chem.* **2004**, *12*, 1305–1314.
(30) (a) Harrick, N. J. *J. Phys. Chem.* **1960**, *64*, 1110–1114. (b) Fahrenfort, J. *Spectrochim. Acta* **1961**, *17*, 698–709.
(31) (a) Eisenberg, D.; Kauzmann, W. *The Structure and Properties of Water*; Oxford University Press: Oxford, U.K., 1969. (b) Rice, S. A.; Bergren, M. S.; Belch, A. C.; Nielson, G. *J. Phys. Chem.* **1983**, *87*, 4295–4308. (c) Belch, A. C.; Rice, S. A. *J. Chem. Phys.* **1983**, *78*, 4817–4823. (d) Buch, V. *J. Phys. Chem. B* **2005**, *109*, 17771–17774.
(32) Köddermann, T.; Schulte, F.; Huelsekopf, M.; Ludwig, R. *Ang. Chem. Int. Ed.* **2003**, *42*, 4904–4908.
(33) Schiffer, J.; Intenzo, M.; Hayward, P.; Calabrese, C. *J. Chem. Phys.* **1976**, *64*, 3014–3020.
(34) Limbach, H. H.; Hennig, J.; Stulz, J. *J. Chem. Phys.* **1983**, *78*, 5432–5436.
(35) Custelcean, R.; Afloroaei, C.; Vlassa, M.; Polverejan, M. *Angew. Chem., Int. Ed.* **2000**, *39*, 3094–3096.
(36) Deshpande, M. S.; Kumbhar, A. S.; Puranik, V. G.; Selvaraj, K. *Cryst. Growth Des.* **2006**, *6*, 743–748.
(37) Lenz, A.; Ojamaee, L. *J. Phys. Chem. A* **2006**, *110*, 13388–13393.
(38) Novak, A. *Hydrogen Bonding in Solids: Correlation of Spectroscopic and Crystallographic Data. Struct. Bonding (Berlin)* **1974**, *18*, 177–216.
(39) Wierzejewska-Hnat, M.; Mielke., Z.; Ratajczak, H. *Spectrochim. Acta* **1987**, *43A*, 675–678.
(40) Evans, J. C. *Spectrochim. Acta* **1960**, *16*, 994–1000.
(41) Rumpel, H.; Limbach, H. H.; Zachmann, G. *J. Phys. Chem.* **1989**, *93*, 1812–1818.
(42) Libowitzky, E. *Monatsh. Chem.* **1999**, *130*, 1047–1059.
(43) Bukowski, R.; Szalewicz, K.; Groenenboom, G. C.; van der Avoird, A. *Science* **2007**, *315*, 1249–1252.
(44) Gerritzen, D.; Limbach, H. H. *Ber. Bunsen-Ges. Phys. Chem.* **1981**, *85*, 527–535.B.

(45) Limbach, H. H.; Seiffert, W. *J. Am. Chem. Soc.* **1980**, *102*, 538–542.
(46) Gerritzen, D.; Limbach, H. H. *J. Am. Chem. Soc.* **1984**, *106*, 869–879.
(47) (a) Sherwood, J. N. Specialist Periodical Report, *Surface and Defect Properties of Solids 2*; Chemical Society: London, 1973; pp 250−268. (b) Sherwood, J. N. *Mol. Cryst. Liq. Cryst.* **1969**, *9*, 37–57. (c) Lockhart, N. C.; Sherwood, J. N. *J. Chem. Soc. Faraday Symp.* **1972**, *6*, 57–65.
(48) Shenderovich, I. G.; Buntkowsky, G.; Schreiber, A.; Gedat, E.; Sharif, S.; Albrecht, J.; Golubev, N. S.; Findenegg, G. H.; Limbach, H. H. *J. Phys. Chem. B.* **2003**, *107*, 11924–11939.
(49) Resing, H. A. *Mol. Cryst. Liq. Cryst.* **1969**, *9*, 101–132.
(50) Titman, J. J.; Luz, Z.; Spiess, H. W. *J. Am. Chem. Soc.* **1992**, *114*, 3756–3 765.
(51) Filsinger, B.; Zimmermann, H.; Haeberlen, U. *Mol. Phys.* **1992**, *76*, 157–172.